# Overview of the Formulation and Numerics of the MIT GCM

**Alistair Adcroft, Chris Hill, Jean-Michel Campin, John Marshall and Patrick Heimbach**

*M.I.T. Climate Modeling Initiative, M.I.T. 54-1624,*
*77 Massachusetts Ave, Cambridge, MA 02139, USA*
*adcroft@mit.edu*

## Abstract

The MIT general circulation model (MITgcm) is a widely portable circulation model designed for study of a wide range of scales in both the ocean and atmosphere. The model is rooted in the incompressible Navier-Stokes equations and can include the non-hydrostatic terms that are important in mixing processes. In the hydrostatic limit, an isomorphism between height based-coordinates and pressure based-coordinates allows the same dynamical kernel to drive an atmospheric model. The model uses finite volume methods and orthogonal curvilinear coordinates in the horizontal that can accommodate novel spherical grids such as that based on the conformally expanded spherical cube. An adjoint of the model is maintained using automatic differentiation.

## 1. Introduction

The MIT general circulation model (MITgcm) was designed from the outset for study of both large-scale/global studies and small-scale processes. MITgcm achieves this capability with various features that have set it apart from most other GCMs, namely a non-hydrostatic capability (Marshall et al., 1997a), the use of the finite volume method in its numerical formulation (Adcroft et al 1997), the maintenance of an automatically generated adjoint (Heimbach et al., 2001), and a layered approach to software and computer technology (Hill et.al.,1999).

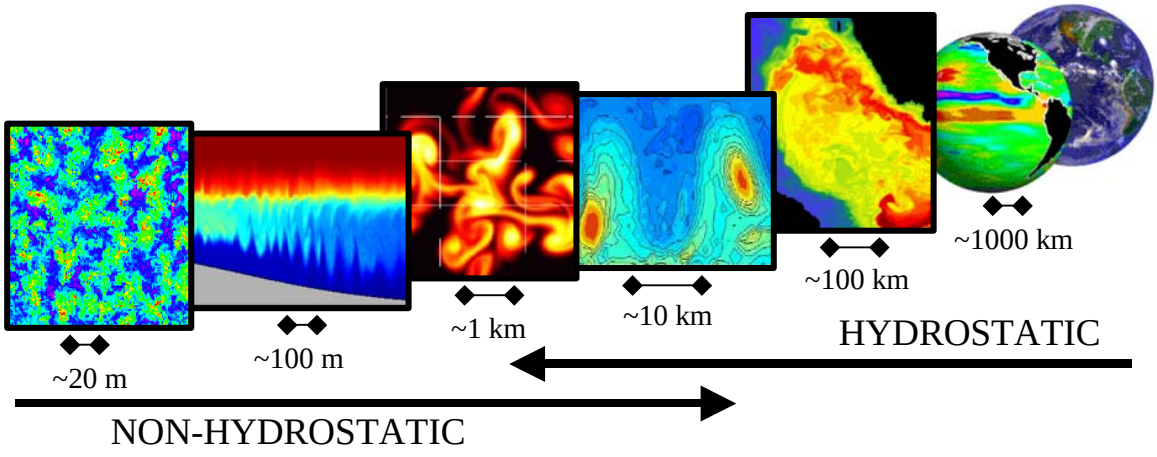


*Figure 1: Schematic of scales on the ocean indicating the grey area where hydrostatic dynamics gives way to non-hydrostatic dynamics.*

The non-hydrostatic capability allows the model to simulate overturning and mixing processes. When used in conjunction with the finite volume representation of topography (known as shaved-cells or partial steps using the method of cut cells) the model provides a flexible tool for studying mixing process and dynamical interactions with steep topography. The adjoint of the model is generated using an adjoint compiler (TAF from FastOpt) and is used in state estimation projects (ECCO: Estimating the Circulation and Climate of the Oceans) as well as numerous sensitivity studies. By exploiting mathematical isomorphisms in the model equations, MITgcm permits atmosphere and ocean general studies with the same set of code and algorithms

(Marshall et al, 2004). The layered approach to writing software means that the model is widely portable and highly efficient on a very wide range of computational platforms (from Macintosh laptops to massively parallel Altix machines).

## 2. Model equations (Marshall et al., 1997a,b)

In the ocean, there is a large separation of time-scales between the fast acoustic modes and the dynamical modes of interest. The speed of sound, $c_s$, is of the order $1500\,\mathrm{ms}^{-1}$ and while typical flow speeds, U, are of order $1\,\mathrm{ms}^{-1}$. In between these scales are the external gravity wave speed, $\sqrt{gH}\sim 150\,\mathrm{ms}^{-1}$ (where H is the fluid depth) and the baroclinic wave speed, $NH\sim 3\,\mathrm{ms}^{-1}$ (assuming a Brunt-Vaisalla, N, frequency of $10^{-4}\mathrm{s}^{-1}$). As a consequence of the large separation between the acoustic scales and those of interest, we can filter the acoustic modes with little approximation and do so by assuming that the flow is incompressible, $D_t\rho << \rho\nabla\cdot\vec{v}$. In addition, density variations in the ocean that arise due to dynamics are typically much smaller than the resting or reference density, $\rho' = (\rho - \rho_o) << \rho_o$, which allows us to use the Boussinesq approximation in which the momentum equations become more linear, $\rho\vec{v} \rightarrow \rho_o\vec{v}$.

The incompressible Boussinesq equations used in the height coordinate mode of the model are

$$\begin{aligned}
\rho_o D_t\vec{v} + 2\Omega\times\rho_o\vec{v} + g\rho\hat{k} + \nabla p &= \vec{F}\\
\rho_o\nabla\cdot\vec{v} &= 0\\
\partial_t\eta + \nabla\cdot(H+\eta)\vec{v}_h &= \text{P-E}\\
D_t\theta &= Q_\theta\\
D_t s &= Q_s\\
\rho &= \rho(s,\theta,p)
\end{aligned}$$

where $\vec{v}$ is the three dimensional velocity vector, p is pressure, $\rho$ is in-situ density, is the displacement of the free-surface from the resting sea-level, $\theta$ is the potential temperature and s is salinity. $\rho_o$ is a constant reference density, g is the constant gravitational acceleration and H is a fixed-in-time bottom depth. $\vec{F}$, P-E, $Q_\theta$, and $Q_s$ are all arbitrary forcing fields which may include sub-grid scale parameterizations. Note that these equations are non-hydrostatic. Most GCM's make the hydrostatic approximation to the vertical momentum equation, in addition to the approximations given above.

## 3. Finite Volume Discretization (Adcroft et al., 1997)

The model is discretized using the finite volume methodology in which the governing equations are integrated over [space-filling] finite volumes that make up a discrete grid. Integrating over a finite volume and applying the Guass-divergence theorem results in a continuity equation of the form

$$A^u_{east}\,u_{east} - A^u_{west}\,u_{west} + A^v_{north}\,v_{north} - A^v_{south}\,v_{south} + A^w_{up}\,w_{up} - A^w_{down}\,w_{down} = 0$$

The area of a cell face describes the geometry of a finite volume and the budget is written conceptually in terms of the normal flow across the cell face; the faces can be curvilinear. The no normal flow at rigid boundaries, $\vec{v}\cdot\hat{n} = 0$, translates to setting the volume flux through a rigid boundary to zero. For example, for the cell depicted in Fig. 2, we would impose $A^w_{down}\,w_{down} = 0$.

It is natural to stagger the components of velocity in the horizontal on an Arakawa C grid and to use a Lorenz grid in the vertical. This places the components most naturally for representing the volume budget terms in the finite volume treatment of the continuity equation.

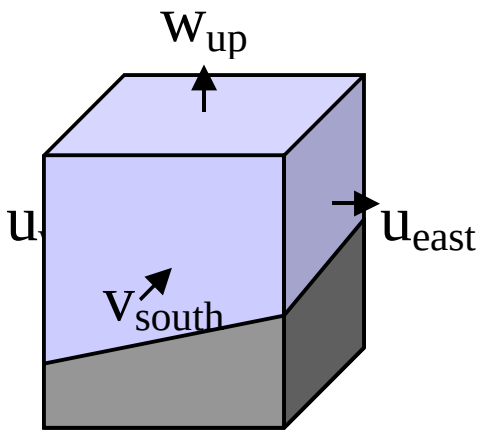


*Figure 2: Schematic of the integrated continuity equation abutting topography.*

The tracer equations are treated in exactly the same manner as the continuity equation and use the same control volumes: using the same volume fluxes for carrying tracer ensures that we conserve tracer by volume.

## 4. Algorithm (Marshall et al., 1997b)

Since the governing equations are incompressible we use the projection method to solve them. Writing the momentum equations, discretized between time levels $^{n}$ and $^{n+1}$, as

$$\rho_o \vec{v}^{n+1} + \Delta t \nabla p = \rho_o \vec{v}^{n} + \Delta t \vec{G} \qquad = \rho_o \vec{v}^{*}$$

we can then substitute into the continuity equation

$$\delta_i (A^u u^{n+1}) + \delta_j (A^v v^{n+1}) + \delta_k (A^w w^{n+1}) = 0$$

to obtain an elliptic equation for pressure

$$\frac{\Delta t}{\rho_o}\left[\delta_i\left(\frac{A^u}{\Delta x}\delta_i p\right)+\delta_j\left(\frac{A^v}{\Delta y}\delta_j p\right)+\delta_k\left(\frac{A^w}{\Delta z}\delta_k p\right)\right] = \delta_i\left(A^u u^*\right)+\delta_j\left(A^v v^*\right)+\delta_k\left(A^w w^*\right)$$

with a seven point stencil.

A three dimensional elliptic equation in an irregular domain can be particularly expensive to solve. To solve this problem we decompose the pressure into dynamical parts: $p = p_s(x,y) + p_h(x,y,z) + p_{nh}(x,y,z)$. Here, $p_s$ is the surface pressure imposed by a rigid-lid (we will discuss the free-surface later) and is constant with depth, $p_h$ is the "hydrostatic" pressure found by integrating hydrostatic balance down from the surface where we impose $p_h(z=0)=0$, and $p_{nh}$ is the remaining part that we call the "non-hydrostatic" pressure perturbation. The surface pressure equation is found following the projection method but here we neglect the unknown terms associated with gradient of non-hydrostatic pressure:

$$\nabla_z \cdot H \nabla_z p_s = \frac{\rho_o}{\Delta t} \nabla \cdot \int_{-H}^{0} (\vec{v}_h^{*} - \Delta t \nabla_z p_h - \Delta t \nabla_z p_{nh}) dz .$$

*neglect here*

We then solve for the "non-hydrostatic" pressure perturbation having found the surface pressure:

$$\nabla^2 p_{nh} = \frac{\rho_o}{\Delta t} \nabla \cdot (\vec{v}^{*} - \Delta t \nabla_z p_s - \Delta t \nabla_z p_h)$$

This equation is un-approximated: if we obtain a poor solution to the surface pressure equation then the non-hydrostatic pressure will compensate. The advantage of this decomposition is that the surface pressure equation is only a two-dimensional elliptic equation and thus much cheaper to solve than the three dimensional problem. It is dominated by larger horizontal scales associated with the barotropic mode and, by solving it, the model propagates information over very large distances. In contrast, solving the three-dimensional perturbation problem, local adjustments remain and so the problem requires many fewer iterations to converge.

The discrete three-dimensional Laplacian operator itself is "stiff": the aspect ratio of the ocean is very small, $H << L$, so that $\nabla_z^2 p_{nh} + \partial_z^2 p_{nh} \approx \frac{1}{\Delta z^2}\delta_{kk} p_{nh}$. This is useful when designing a pre-conditioner for the conjugate gradient algorithm used to solve the elliptic problem iteratively. The pre-conditioner involves solving a tri-diagonal problem in the vertical which can be solved very efficiently and also dictates that we only decompose horizontally for parallel machines.

The thermodynamic variables are integrated forward using a "staggered" algorithm:

$$
\begin{aligned}
\theta^{n+\frac{1}{2}} &= \theta^{n-\frac{1}{2}} + \Delta t\left(Q_\theta{}^n - \nabla\cdot F(\vec{v}^n,\tilde{\theta})\right)\\
s^{n+\frac{1}{2}} &= s^{n-\frac{1}{2}} + \Delta t\left(Q_s{}^n - \nabla\cdot F(\vec{v}^n,\tilde{s})\right)\\
\rho^{n+\frac{1}{2}} &= \rho\left(s^{n+\frac{1}{2}},\theta^{n+\frac{1}{2}},p_o(z)\right)\\
p_h^{n+\frac{1}{2}} &= -\int_z^0 g\rho^{n+\frac{1}{2}}dz'\\
\vec{v}* &= \vec{v}^n + \Delta t\left(G(\tilde{\vec{v}}) + F^{n+\frac{1}{2}} - \nabla_z p_h^{n+\frac{1}{2}}\right)\\
\nabla^2 p_{nh} &= \nabla\cdot\vec{v}*\\
\vec{v}^{n+1} &= \vec{v}* - \Delta t\nabla p_{nh}
\end{aligned}
$$

The last three lines correspond to the projection method described above. The advantage of staggering is that it treats the gravity wave terms as centered in time and has the stability of a leap-frog scheme for those modes but at half of the cost. It also naturally centers the advective flow field in time for the purposes of transporting tracers.

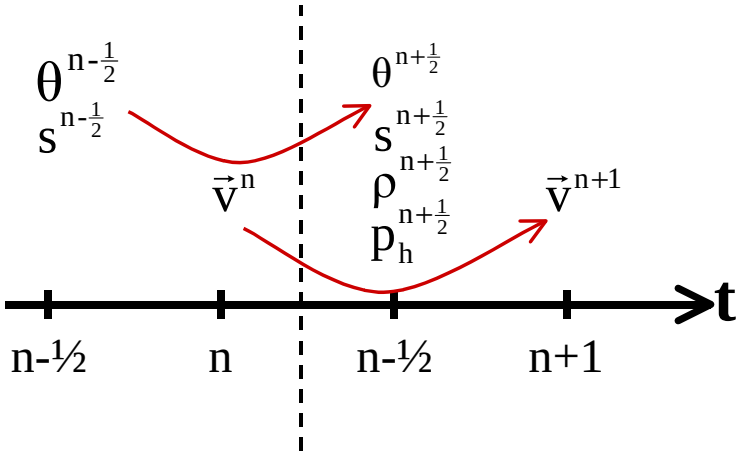


*Figure 3 Schematic of the staggered algorithm where thermodynamic variables are staggered in time with the flow variables.*

# 5. Free-surface treatment (Campin et al., 2004)

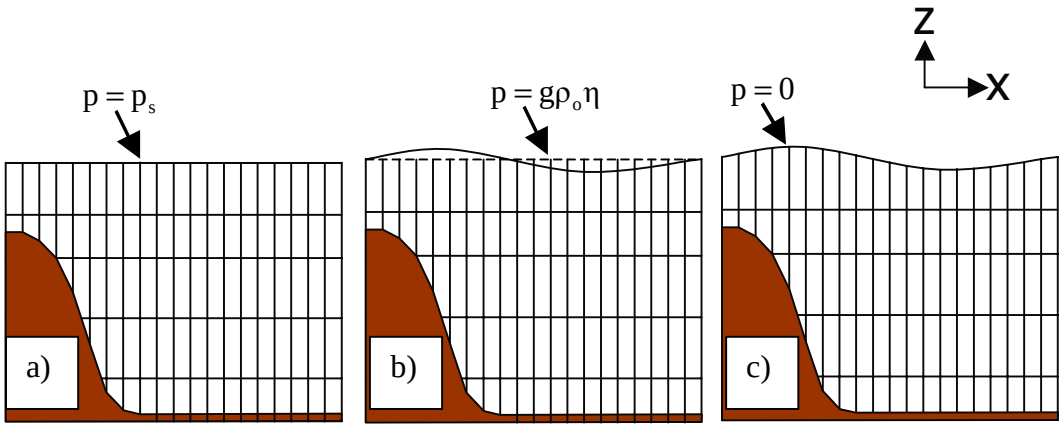


*Figure 4: Three forms of the upper surface treatment: (a) the rigid-lid approximation which imposes a pressure on the fluid, (b) the linear free-surface which permits shallow water waves to propagate but uses a fixed geometry and (c) the non-linear free-surface which makes no approximation to the upper boundary and have time-dependent finite volumes for the upper layer.*

The upper surface of the ocean is a free surface which is driven by the divergence of volume flux (Boussinesq) in the interior. There are three treatments of the upper boundary available in MITgcm:

1. Rigid-lid approximation in which the upper surface is imagined to be an impermeable boundary which exerts a pressure on the fluid. This pressure is constructed so as to guarantee that the depth integrated divergence of the volume flux is zero: $\nabla \cdot \int_{-H}^{0} \vec{v}\, dz = 0$
2. The linear free-surface which ignores some small terms in the depth integrated continuity equation, $\partial_t \eta + \nabla \cdot \int_{-H}^{0} \vec{v} dz = P - E$. This permits surface gravity waves to propagate with finite phase speed and introduces a Helmholtz term in the surface pressure equation when treated implicitly in time. This is a very good approximation in deep water for which $\eta << H$.
3. The non-linear free-surface is an un-approximated treatment of the upper surface: $\partial_t \eta + \nabla \cdot \int_{-H}^{\eta} \vec{v} dz = P - E$. This involves the same algorithm as in the linear free-surface but with explicit treatment of the additional non-linear terms. The major impact on the model is that the geometry of the upper level finite volumes is now time dependent.

Although the last option involves no approximations, it has limitations due to a practical issue of accuracy when the free-surface variations become large with respect to the vertical resolution. Indeed, when $|\eta| \sim \Delta z_1$ then the upper layer can vanish and out-crop the second layer.

# 6. Coordinates and Isomorphisms

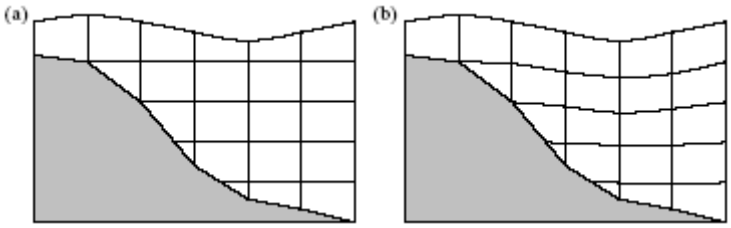


*Figure 5: Schematic of (a) height coordinates with a finite volume treatment of the upper layer and topography and (b) z* coordinates with a finite volume treatment of topography.*

To avoid the vanishing layer problem associated with the non-linear free-surface we employ a modified height coordinate, z*, that is stretched so that the model's upper computational boundary tracks the physical free-surface (Adcroft et al., 2004). The coordinate transformation is given by

$$z^* = \frac{z-\eta}{H+\eta} H$$

so that at the solid bottom

$$\begin{pmatrix} z = -H \\ w = -\vec{v}_h \cdot \nabla H \end{pmatrix} \Leftrightarrow \begin{pmatrix} z^* = -H \\ w^* = -\vec{v}_h \cdot \nabla H \end{pmatrix}$$

and at the free-surface

$$\begin{pmatrix} z = \eta \\ w = D_t \eta - (P-E) \end{pmatrix} \Leftrightarrow \begin{pmatrix} z^* = 0 \\ w^* = \frac{-H}{H+\eta}(P-E) \end{pmatrix}$$

The z* coordinate deviates only slightly from height because $|\eta| << |H|$ and so it should be thought of as a height coordinate that is slightly stretched to follow the motions of the external mode. The hydrostatic equations in z* coordinates are

$$\rho_o D_t^* \vec{v}_h + f\hat{k} \times \rho_o \vec{v} + \nabla_{z^*} p + \rho \nabla_{z^*} \Phi = \vec{F}_h$$
$$\partial_{z^*} p + \left(\frac{H+\eta}{H}\right) g\rho = 0$$

$$\partial_t \left(\frac{H+\eta}{H}\right) + \nabla_{z^*} \cdot \left(\frac{H+\eta}{H} \vec{v}_h\right) + \partial_{z^*} \left(\frac{H+\eta}{H} w^*\right) = 0$$
$$\partial_t \eta + \nabla \cdot \int_{-H}^{0} \frac{H+\eta}{H} \vec{v}_h \, dz^* = P\text{-}E$$

$$\partial_t \left(\frac{H+\eta}{H}\theta\right) + \nabla_{z^*} \cdot \left(\frac{H+\eta}{H}\theta \vec{v}_h\right) + \partial_{z^*} \left(\frac{H+\eta}{H}\theta w^*\right) = Q_\theta$$

$$\partial_t \left(\frac{H+\eta}{H} s\right) + \nabla_{z^*} \cdot \left(\frac{H+\eta}{H} s \vec{v}_h\right) + \partial_{z^*} \left(\frac{H+\eta}{H} s w^*\right) = Q_s$$

in which there are now two pressure gradient terms in the horizontal momentum equations and thus the possibility of pressure gradient errors arise. However, unlike in terrain following coordinates, where the slope of coordinate surfaces can be steep, the slope of z* surfaces is very small because $|\nabla\eta| << |\nabla H|$.

The height coordinate hydrostatic equations describing the incompressible, Boussinesq ocean are isomorphic with the pressure coordinate hydrostatic equations describing the compressible non-Boussinesq atmosphere

(Marshall et al., 2004; Losch et al., 2003). That is to say, the equations and boundary conditions look similar in form and that the vertical coordinate and variables can be re-interpreted between the two fluids.

$$
\begin{aligned}
D_t\vec{v}_h + f\hat{k}\times\vec{v}_h + \nabla_p\Phi &= \vec{F} \\
\partial_p\Phi + \alpha &= 0 \\
\nabla_p\cdot\vec{v}_h + \partial_p\omega &= 0 \\
\partial_t p_s + \nabla\cdot p_s\langle\vec{v}_h\rangle &= 0 \\
D_t\theta &= Q_\theta \\
D_t q &= Q_q \\
\alpha &= \tfrac{\partial\Pi}{\partial p}\theta
\end{aligned}
$$

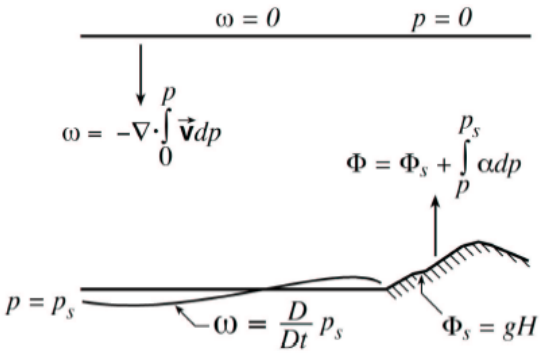


*Figure 6: Schematic of the boundary conditions and direction of vertical integrations in the pressure coordinate atmospheric model.*

$$
\begin{aligned}
D_t\vec{v}_h + f\hat{k}\times\vec{v}_h + \tfrac{1}{\rho_o}\nabla_z p &= \vec{F} \\
\partial_z p + g\rho &= 0 \\
\nabla_z\cdot\vec{v}_h + \partial_z w &= 0 \\
\partial_t\eta + \nabla\cdot(H+\eta)\vec{v}_h &= P - E \\
D_t\theta &= Q_\theta \\
D_t s &= Q_s \\
\rho &= \rho(s,\theta,p)
\end{aligned}
$$

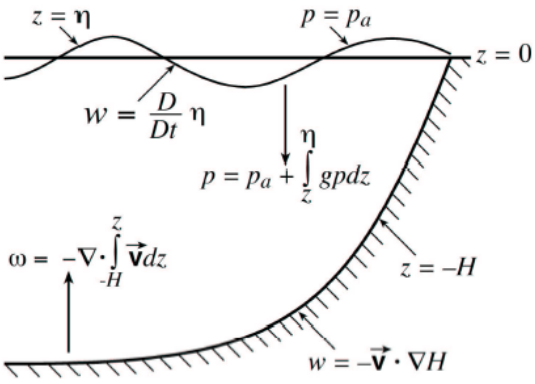


*Figure 7: Schematic of the boundary conditions and direction of vertical integrations in the height coordinate oceanic model.*

The isomorphism between atmospheric and oceanic equations allows us to use the same dynamical kernel to drive either the ocean or atmosphere. We discriminate between the two fluids by using the appropriate equation of state, forcing and parameterizations. Algorithmically, the models are identical and the isomorphism applies to the boundary conditions also, although some appear homogenous in one fluid while inhomogeneous in the other. This allows the MITgcm to be applied to the atmosphere and ocean and has motivated new developments that might not have occurred if the model were being applied to just the ocean.

The z-p isomorphism has analogs for other coordinate pairs, for instance, height based terrain following coordinates are isomorphic with the pressure based terrain-following coordinate of Philips. Another is the z*-p* isomorphism where p* is the “eta” coordinate of Mesinger, 1988. That is, the advantages and ideas developed in the z* coordinate also apply to the atmospheric analog, p*.

## 7. Finite volume advection

The tracer equations are discretized using the finite volume method described earlier in that the cell can be arbitrarily shaped to fit topography. The fluxes are calculated using the finite volume method which involves a polynomial fitting that conserves the volume integral of moments. The advective flux can be interpreted as

that volume of fluid that passes through the cell interface; this gives an upstream bias for odd order polynomials. For the one-dimensional advection problem, $\partial_t\theta = -u\partial_x\theta = -\partial_x F$, the discrete fluxes are

$$F^{US}_{i+½} = u\theta^n_i$$

$$F^{LW}_{i+½} = F^{US}_{i+½} + \tfrac{1}{2}u(1\text{-}C)\left(\theta^n_{i+1} - \theta^n_i\right)$$

$$F^{DST3}_{i+½} = F^{LW}_{i+½} - \tfrac{1}{6}u(1-C^2)\left(\theta^n_{i+1} - 2\theta^n_i + \theta^n_{i-1}\right)$$

where $C = \dfrac{\Delta t u}{\Delta x}$ is the Courant number.

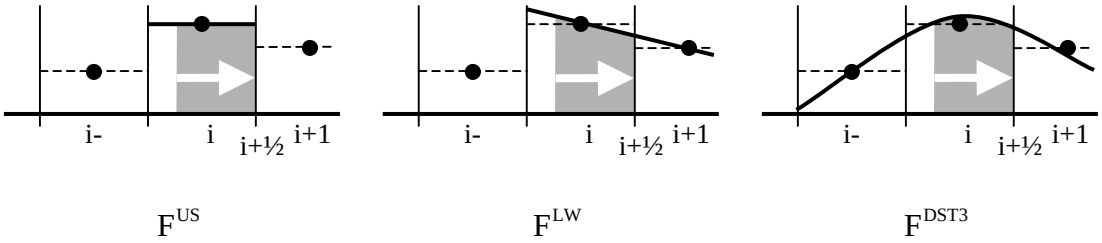


*Figure 8: The finite volume method representation of advection at three orders of accuracy. The polynomial are constructed to recover volume integrals of moments and the flux is found by integrating the over the control volume that is swept through the interface.*

The resulting tracer equations are accurate to n'th order in both time and space due to a cancellation of space-time truncation errors in the manner of the Lax-Wendroff scheme:

$$\begin{aligned}
\frac{1}{\Delta t}\left(\theta^{n+1}_i - \theta^n_i\right) + \frac{1}{\Delta x}\left(F^{US}_{i+½} - F^{US}_{i-½}\right) &= \partial_t\theta + u\partial_x\theta \quad + O(\Delta t, \Delta x) \\
\frac{1}{\Delta t}\left(\theta^{n+1}_i - \theta^n_i\right) + \frac{1}{\Delta x}\left(F^{LW}_{i+½} - F^{LW}_{i-½}\right) &= \partial_t\theta + u\partial_x\theta \quad + O(\Delta t^2, \Delta x^2). \\
\frac{1}{\Delta t}\left(\theta^{n+1}_i - \theta^n_i\right) + \frac{1}{\Delta x}\left(F^{DST3}_{i+½} - F^{DST3}_{i-½}\right) &= \partial_t\theta + u\partial_x\theta \quad + O(\Delta t^3, \Delta x^3)
\end{aligned}$$

These fluxes can subsequently be limited to ensure monotonicity and avoid spurious extrema (Hundsorfer and Trompert, 1994). The one-dimensional methods are extended to three dimensions by removing the local divergence of the flow in each dimension:

$$\begin{aligned}
\theta^{n+⅓} &= \theta^n - \Delta t\left[\partial_x\left(u\theta^n\right) - \theta^n\partial_x u\right] \\
\theta^{n+⅔} &= \theta^{n+⅓} - \Delta t\left[\partial_y\left(v\theta^{n+⅓}\right) - \theta^n\partial_y v\right] \\
\theta^{n+1} &= \theta^{n+⅔} - \Delta t\left[\partial_z\left(w\theta^{n+⅔}\right) - \theta^n\partial_z w\right] \\
\theta^{n+1} &= \theta^{n+⅔} - \Delta t\theta^n\left(\partial_x u - \partial_y v - \partial_z w\right)
\end{aligned}.$$

The essential idea here is that one dimensional methods assume non-divergent flow but three-dimensional flow appears divergent in any one direction. The method above removes the divergent part of the flow by using the identity $u\partial_x\theta = \partial_x(u\theta) - \theta\partial_x u$. The divergent contribution is added back in at the end so that the system is still conservative. This approach avoids the shape deforming problems that arise when one-dimensional methods are naively applied in each direction independently.

# 8. Gridding the sphere (Adcroft et al., 2004)

A long standing problem of grid-point models on the sphere is that of converging meridians (the pole problem). The convergence of meridians implies very small zonal grid elements which can lead to severe restrictions on explicit time-steps. In a conventional geographic coordinate grid (latitude-longitude), the smallest element length scales as $\Delta x_{\min} \sim N^{-2}$, where N is the number of points around the equator. This means that doubling the number of points halves the resolution at the equator but quarters the resolution near the poles. MITgcm can use another gridding of the sphere such as those based on the conformally expanded spherical cube of Rancic et al., 1996. This grid has much improved scaling, $\Delta x_{\min} \sim N^{-4/3}$, which allows it to be taken to much higher resolution before becoming prohibitive and provides much more uniform coverage of the sphere.

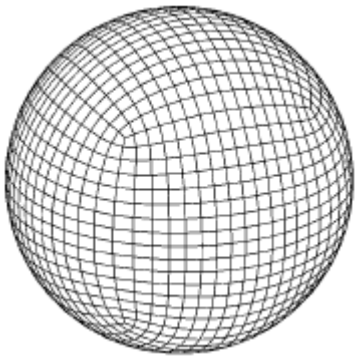

*Figure 9: An example of the conformally expanded spherical cube grid.*

The grid is orthogonal curvilinear but has eight singularities where the coordinates and flow variables become degenerate. Writing the model equations in tensorial form and evaluating terms involving components of vectors often places quantities on these singularities. An example is the evaluation of the relative vorticity on a corner with a C grid staggering of variables.

The solution to this problem is to use the finite volume method and integral form of quantities. In the case of vorticity, the circulation around the corner singularity is unambiguously defined and calculable and invariant with respect to the tile. The equations best suited for this approach are the vector invariant equations written:

$$
\begin{aligned}
\partial_t u - (f+\zeta) v + w\partial_z u + \partial_x\left(K + \tfrac{1}{\rho_o} p\right) &= F_u \\
\partial_t v + (f+\zeta) u + w\partial_z u + \partial_y\left(K + \tfrac{1}{\rho_o} p\right) &= F_v \\
g\rho + \partial_z p &= 0 \\
\partial_x u + \partial_y v + \partial_z w &= 0 \\
\partial_t \theta + \partial_x (u\,\theta) + \partial_y (v\,\theta) + \partial_z (w\,\theta) &= Q
\end{aligned}
$$

We discretize these equations as follows:

$$
\begin{aligned}
\Delta z \Delta y_u \left[ \Delta x_u \partial_t u - \overline{f+\zeta}^{\,j} \overline{\overline{\Delta x_v v}^{\,j}}^{\,i} + \delta_i\left(K + \tfrac{1}{\rho_o} p\right) \right] + \overline{\overline{Aw}^{\,i}}^{\,k} \delta_k u &= \Delta z \Delta y_u \Delta x_u F_u \\
\Delta z \Delta x_v \left[ \Delta y_v \partial_t v - \overline{f+\zeta}^{\,i} \overline{\overline{\Delta y_u u}^{\,i}}^{\,j} + \delta_j\left(K + \tfrac{1}{\rho_o} p\right) \right] + \overline{\overline{Aw}^{\,j}}^{\,k} \delta_k v &= \Delta z \Delta x_v \Delta y_u F_v \\
g \overline{\Delta z \rho}^{\,k} + \delta_k p &= 0 \\
\delta_i(\Delta z \Delta y_u u) + \delta_j(\Delta z \Delta x_v v) + \delta_k(Aw) &= 0 \\
\Delta z A \partial_t \theta + \delta_i(\Delta z \Delta y_u u \theta) + \delta_j(\Delta z \Delta x_v v \theta) + \delta_k(Aw\theta) &= \Delta z A Q
\end{aligned}
$$

There still remain terms that involve components of flow variables (namely the non-linear Coriolis terms). Here, we note that the order in which operators are applied is important; we have ordered the interpolation operators so as to interpolate via cell centers and not cell corners. The average operators can no longer be assumed to commute near singularities, $\overline{\overline{u}^{j}}^{i} \neq \overline{\overline{u}^{i}}^{j}$. Avoiding commuting operators and using the finite volume method allows the use of grids with singularities in a robust manner.

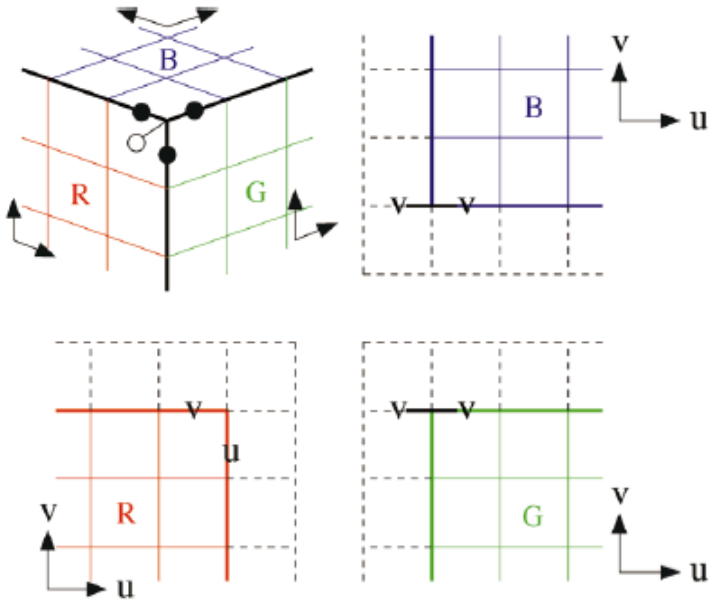


*Figure 10: Components of the horizontal flow vector required to evaluate the relative vorticity on a corner singularity of the cubed grid. The answer can depend on the perspective of the face/tile for which the calculation is being made. There is no choice of interpolation for the flow components that gives the same answer on all tiles for all terms.*

## 9. Summary

We have presented an overview of the design of the MITgcm. We have only discussed the essential aspects of the kernel and not mentioned the numerous options that allow different numerical and algorithmic treatments. The model has been demonstrated to work over a wide range of scales. To achieve this capability

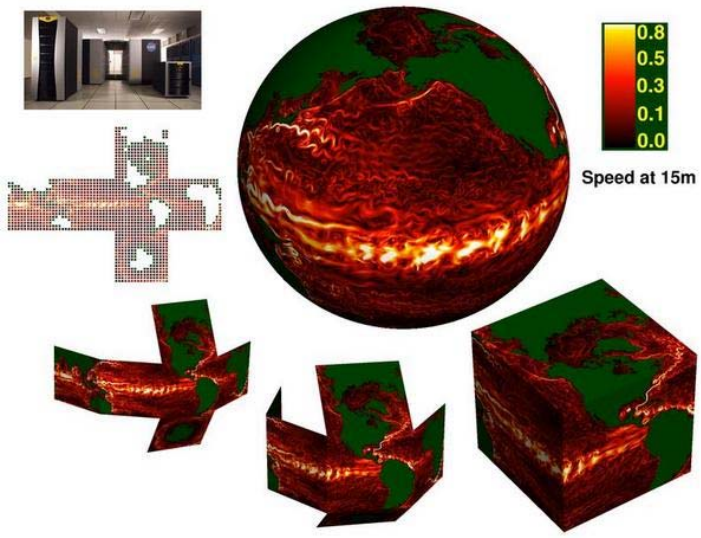


*Figure 11: An eddy-permitting calculation of the global ocean. Shown in colors is the current speed at 15 m depth. The calculation was carried out on 480 Altix processors at NASA/AMES and conducted by D. Menemenlis and Chris Hill under the auspices of ECCO.*

many innovations have been made that were originally motivated by applications at one scale but turn out to be beneficial at other scales. Similarly, our isomorphic approach has directed model development down a path that we might not have followed if we were targeting just the ocean. The end result is a uniquely versatile model that can be applied to a wide range of problems in both the ocean and atmosphere.

## 10. References and further reading

Adcroft, A. and J.-M. Campin, 2004: Rescaled height coordinates for accurate representation of free-surface flows in ocean circulation models. *Ocean Modelling*. **7**, 269-284.

Adcroft, A., J.-M. Campin, C.N. Hill and J.C. Marshall, 2004: Implementation of an atmosphere-ocean general circulation model on the expanded spherical cube. *Month. Weath. Rev.*, in press.

Adcroft, A., C. Hill and J. Marshall, 1997: The Representation of Topography by Shaved Cells in a Height Coordinate Model. *Month. Weath. Rev.* **125** (9), 2293-2315.

Campin, J.-M., A. Adcroft, C. Hill and J. Marshall, 2004: Conservation of properties in a free-surface model. *Ocean Modelling*. **6**, 221-244.

Heimbach, P., C. Hill and R. Giering, 2002: Automatic Generation of Efficient Adjoint Code for a Parallel Navier-Stokes Solver. J.J. Dongarra, P.M.A. Sloot and C.J.K. Tan (Eds.), Lecture Notes in Computer Science (LNCS), Vol. 2330, part II, pp. 1019-1028, Springer-Verlag.

Hill, C., A. Adcroft, D. Jamous and J. Marshall, 1999: A strategy for terascale climate modeling. In In Proc. of the 8th ECMWF Worksh. on the Use of Parallel Processors in Meteorology, pages 406-425.

Hundsdorfer, W., and R.A. Trompert, 1994: Method of lines and direct discretization: a comparison for linear advection. *App. Numer. Math.* **13**, 469-490.

M. Losch, A. Adcroft and J.-M. Campin, 2003: How sensitive are Coarse General Circulation Models to Fundamental Approximations in the Equations of Motion? *J. Phys. Oceanogr.* **34** (1), 306-319

Marshall, J. A. Adcroft, J-M Campin, C. Hill and A. White, 2004: Atmosphere-ocean modeling exploiting fluid isomorphisms. In press *Month. Weath. Rev.*

Marshall, J., A. Adcroft, C. Hill, L. Perelman and C. Heisey, 1997: A finite-volume, incompressible Navier Stokes model for studies of the ocean on parallel computers. *J. Geophys. Res.* **102** (C3), 5753-5766.

Marshall, J., C. Hill, L. Perelman, C. Heisey and A. Adcroft, 1997: Hydrostatic, quasi-hydrostatic and nonhydrostatic ocean modeling. *J. Geophys. Res.* **102** (C3), 5733-5752.

Mesinger, F., Jancic, Z. I., Mickovic, S., Gavrilov, D., 1988. The Step-Mountain Coordinate: Model Description and Performance for Cases of Alpine Lee Cyclogenesis and for a Case of an Appalachian Redevelopment. *Mon. Wea. Rev.*, **116**, 1493-1518.

Rancic, M., R. J. Purser, and F. Mesinger, 1996: A global shallowwater model using an expanded spherical cube: Gnomonic versus conformal coordinates. *Quart. J. Roy. Meteor. Soc.*, **122,** 959–982.